OPEN

NPG Asia Materials (2016) 8, e274; doi:10.1038/am.2016.65
www.nature.com/am

ORIGINAL ARTICLE

Electronic spin transport in dual-gated bilayer graphene

Ahmet Avsar[1], Ivan Jesus Vera-Marun[2], Jun You Tan[1], Gavin Kok Wai Koon[1], Kenji Watanabe[3], Takashi Taniguchi[3], Shaffique Adam[1,4] and Barbaros Özyilmaz[1,5]

The elimination of extrinsic sources of spin relaxation is key to realizing the exceptional intrinsic spin transport performance of graphene. Toward this, we study charge and spin transport in bilayer graphene-based spin valve devices fabricated in a new device architecture that allows us to make a comparative study by separately investigating the roles of the substrate and polymer residues on spin relaxation. First, the comparison between spin valves fabricated on SiO_2 and BN substrates suggests that substrate-related charged impurities, phonons and roughness do not limit the spin transport in current devices. Next, the observation of a fivefold enhancement in the spin-relaxation time of the encapsulated device highlights the significance of polymer residues on spin relaxation. We observe a spin-relaxation length of ~ 10 μm in the encapsulated bilayer, with a charge mobility of 24 000 $cm^2 Vs^{-1}$. The carrier density dependence on the spin-relaxation time has two distinct regimes; $n < 4 \times 10^{12}$ cm^{-2}, where the spin-relaxation time decreases monotonically as the carrier concentration increases, and $n \geqslant 4 \times 10^{12}$ cm^{-2}, where the spin-relaxation time exhibits a sudden increase. The sudden increase in the spin-relaxation time with no corresponding signature in the charge transport suggests the presence of a magnetic resonance close to the charge neutrality point. We also demonstrate, for the first time, spin transport across bipolar p–n junctions in our dual-gated device architecture that fully integrates a sequence of encapsulated regions in its design. At low temperatures, strong suppression of the spin signal was observed while a transport gap was induced, which is interpreted as a novel manifestation of the impedance mismatch within the spin channel.

NPG Asia Materials (2016) **8,** e274; doi:10.1038/am.2016.65; published online 3 June 2016

INTRODUCTION

Graphene is considered to be a promising spin-channel material for future spintronics applications[1] because of its high-electronic mobility,[2] weak spin–orbit coupling[3,4] and a negligible hyperfine interaction.[5,6] The initial spin transport studies were mainly performed on single-layer[7–10] and bilayer exfoliated graphene,[9,11] and large-area graphene[12–15] deposited on conventional SiO_2 substrates. Although enhanced spin-relaxation times have been reported for bilayer graphene-based devices compared with those based on a single layer, the relatively low spin diffusion constants overall yield a lower spin-relaxation length of only 1–2 μm,[9,11] far below the theoretical predictions.[16] One approach suggested for achieving a longer distance spin communication is to increase the spin diffusion constants by fabricating higher mobility devices.[8,17]

For charge transport, it has been shown that the carrier mobility of graphene devices on SiO_2 is mainly limited by interfacial charged impurities, surface roughness, and phonons.[18–20] The demonstration of an order-of-magnitude improvement in the mobility of graphene encapsulated between atomically flat, charge trap free boron nitride crystals[21,22] has triggered the recent spin transport studies in encapsulated single layer and recently bilayer graphene-based spin valves, where a spin-relaxation length of up to ~ 12 μm and ~ 24 μm have been observed, respectively.[23,24] For the case of bilayer graphene, the initial experiments on SiO_2 revealed an inverse scaling between spin and momentum relaxation times, for example, the longest spin-relaxation times were observed in the lowest-mobility devices.[9,11] Within the standard picture of the spin-relaxation mechanism, such scaling was interpreted as the dominance of a Dyakonov–Perel type scattering mechanism[25] in bilayer graphene-based spin valves on SiO_2. Nevertheless, the strength of the extracted spin–orbit coupling was one order of magnitude higher than the theoretical predictions, which brings into question this standard interpretation.[26] Recently, Kochan *et al.*[27,28] proposed a new spin-relaxation mechanism beyond the standard picture for both single-layer and bilayer graphene driven by resonant scattering that is due to a low concentration of magnetic impurities. For the testing of this theory, bilayer graphene is a more ideal platform because a non-monotonic correlation is predicted for the energy dependence of the spin-relaxation time in the bilayer graphene case that can be experimentally verified.[27] Ultimately, a similar mobility enhancement in bilayer graphene may be a successful

[1]Centre for Advanced 2D Materials, National University of Singapore, Singapore, Singapore; [2]School of Physics and Astronomy, University of Manchester, Manchester, UK; [3]Advanced Materials Laboratory, National Institute for Materials Science, Tsukuba, Japan; [4]Yale-NUS College, 16 College Avenue West, Singapore, Singapore and [5]Department of Physics, National University of Singapore, Singapore, Singapore
Correspondence: Dr A Avsar or Professor B Özyilmaz, Department of Physics, National University of Singapore, 2 Science Drive 3, S13-02-10, Singapore 117542, Singapore.
E-mail: aavsar@gmail.com or barbaros@nus.edu.sg
Received 6 November 2015; revised 2 February 2016; accepted 16 February 2016

route to enhance the spin-relaxation lengths, although this is strongly dependent on the scattering source and the mechanism of spin relaxation.[27,29–31]

MATERIALS AND METHODS

Preparation of the devices

In this article, we discuss the charge and spin transport in high-mobility bilayer graphene-based spin valve devices, using a novel device architecture that overcomes the current technological limit of having a single encapsulated region.[23,24] To understand the effect of the substrate and polymer residues on spin relaxation, we fabricated three types of bilayer graphene spin valve devices in a single sample. (1) A spin valve on SiO_2, (2) a spin valve on BN and (3) an encapsulated spin valve between a BN substrate and a pre-patterned BN strip. The schematics for the fabrication of the encapsulated spin valve devices are shown in Figure 1a. The fabrication starts with the transfer of a bilayer graphene onto atomically flat BN crystals by utilizing the standard dry-transfer method.[32] To create uniform and ultra-clean interfaces, the graphene on the BN substrate is first etched with an O_2 plasma into a 1-μm width strip in the bubble- and wrinkle-free regions of the stack and then annealed at 340 °C for 6 h under an Ar/H_2 gaseous mixture (Figure 1b). This annealing process minimizes the fabrication residues that form during the etching processes. Meanwhile, a second BN layer is exfoliated onto an SiO_2 (300 nm)/Si wafer and then patterned into BN strips by e-beam lithography and etching (CHF_3–O_2–, 10:1 ratio) processes (Figure 1c). This pre-patterned BN layer, a novel aspect in our device architecture, is isolated from the wafer with a KOH etching process and finally transferred onto the previously prepared BLG/BN stack, as shown in Figure 1d. The final stack is annealed under the same conditions as above. The fabrication is completed by forming MgO/Co/Ti (2.2 nm/30 nm/5 nm) electrodes on top of both the BN strips and the non-encapsulated regions of the graphene strip (Figure 1e); these serve as top gate electrodes and direct-contact electrodes to bilayer graphene, respectively. The width of the contact electrodes was varied from 300 nm to 1 μm to ensure the different coercive fields to switch the relative polarization directions of the ferromagnetic electrodes during spin transport measurements. The distance between the edges of adjacent contacts is ~ 3 μm, and the width of the encapsulating BN strip is 2.5 μm. The details for the fabrication of the MgO barrier layer are discussed in the Supplementary Information S1. Although an annealing process after metallization is a standard procedure to achieve very high mobilities in graphene-based heterostructure devices,[18,19] we omitted this process because of the degradation of the ferromagnetic electrodes during annealing (Supplementary Figure S5).[8] The pre-patterned top BN layer therefore adds a new degree of freedom to the device architecture. It allows one to easily design a series of encapsulated regions with arbitrary lengths, whereas the non-encapsulated regions destined for the contacts can be scaled down to the lower precision limit of the lithography technique. This represents a technological improvement over the approach prevalent in the literature, which is limited in practice to a single encapsulated region.[23,24]

Electrical measurements of the devices

Measurements are carried out with standard a.c. lock-in techniques at low frequencies using the local four-terminal setup for charge transport measurements and the non-local setup for spin transport measurements (Figure 1a). In the local charge transport measurements, the current flows between electrode *1* and electrode *4* and a local voltage drop is measured between electrode *2* and electrode *3*. In the non-local measurement configuration, the current flows between the pair of electrodes *1* (injector) and *2*, and a non-local voltage is recorded across the neighboring pair of electrodes *3* (detector) and *4*. SiO_2 and BN dielectrics are utilized to apply back and top gate biases (V_{BG} and V_{TG}), respectively. Unless otherwise stated, electrode *6* is used to locally tune the carrier type and concentration (Supplementary Figure S4). All transport measurements are performed under vacuum (~1×10^{-6} Torr). In this work, we have characterized a total of five junctions in two separate samples (Samples A and B). The bilayer graphene in Sample A has both encapsulated and non-encapsulated junctions, allowing a direct comparison of the charge and spin transport in both cases (Supplementary Figure S1). An optical image of the completed Sample B is shown in Figure 1e.

RESULTS AND DISCUSSION

We first discuss the room temperature spin transport results of the non-encapsulated device, Sample A, at $V_{BG}=0$ V. The relative magnetization directions of the Co electrodes are altered by sweeping the in-plane magnetic field along their easy axis. This changes the spin accumulation between the injector and detector electrodes and leads to a non-local spin signal with a change in resistance, ΔR, of ~ 0.3 Ω (Figure 2a). We note that the observed spin signal is comparable with earlier reports[11,12,33] (Supplementary Figure S6). To confirm the origin of the spin signal and extract the important spin parameters, we performed Hanle spin precession measurements. For this purpose, the magnetization directions of the injector and detector electrodes are made parallel to each other by the application of an in-plane magnetic field. This is followed by sweeping the magnetic field perpendicular to the graphene plane forcing the spins to precess (Figure 2b). The obtained spin precession data are fitted with the solution to the Bloch equation, $R_{NL} \sim \int_O^\infty \frac{1}{\sqrt{4\pi D_S t}} \exp(\frac{-L^2}{4D_S t}) \exp(\frac{-t}{\tau_S}) \cos(w_L t) dt$, where L (≈1.7 μm) is the separation between the electrodes (center-to-center distance), and ω_L is the Larmor frequency. This gives a spin-relaxation time (τ_S) of ~ 87 ps, a spin diffusion constant (Ds) of ~ 0.02 $m^2\,s^{-1}$,

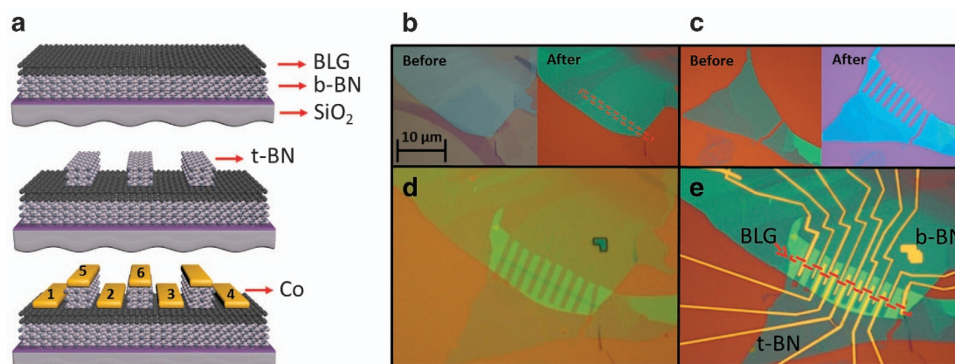

Figure 1 Device characterization. (**a**) A schematic of the device preparation. (**b**) Bilayer graphene is first transferred to the top of a BN layer, and this step is followed by the etching of graphene into a strip. (**c**) Next, a second BN layer is exfoliated onto a standard wafer and patterned into strips. (**d**) Then, the second transfer is completed by encapsulating the bilayer graphene on BN with the pre-patterned BN. The image is captured after spin coating with PMMA to enhance the contrast of graphene. (**e**) Finally, ferromagnetic tunnel contacts are formed under ultra-high vacuum conditions.

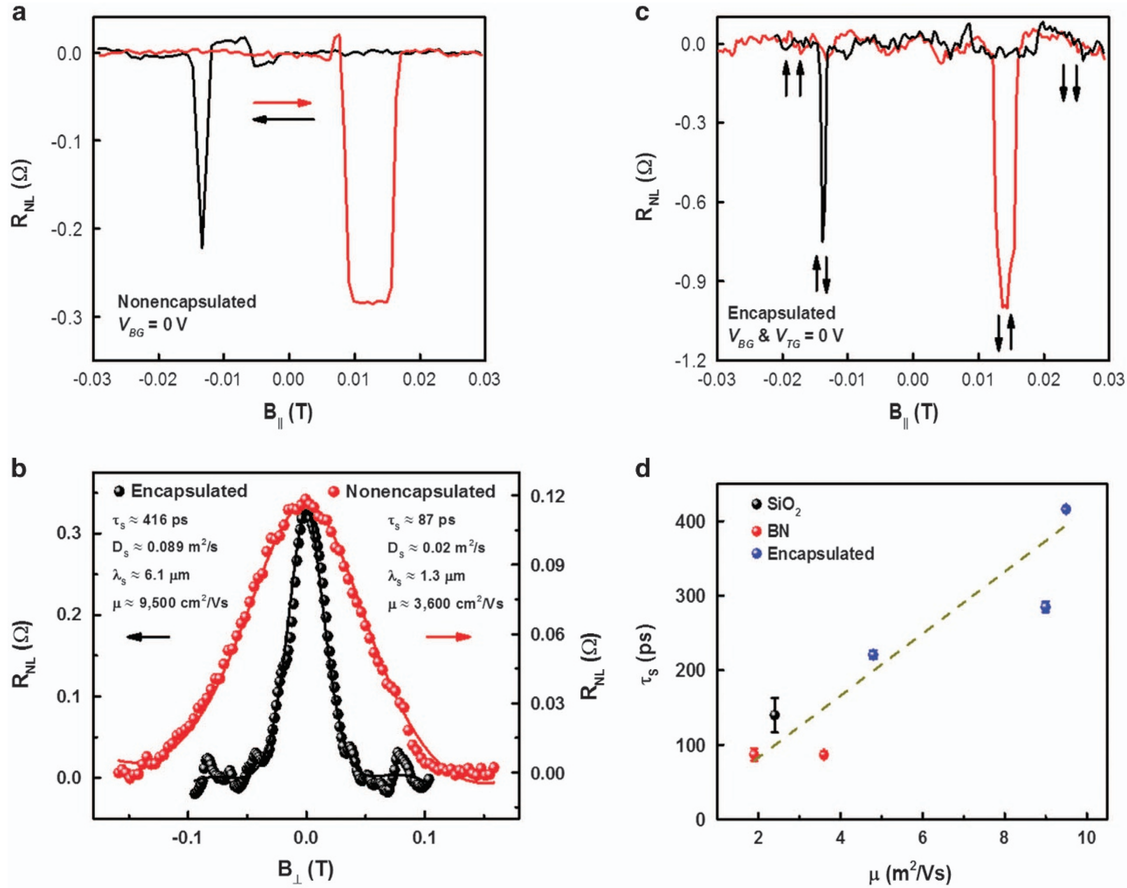

Figure 2 Room temperature electronic spin transport measurements at $V_{BG}= V_{TG}=0$ V. (**a**, **b**) The spin transport and spin precession measurements for the bilayer graphene device fabricated on the BN substrate. (**b**, **c**) The spin transport and spin precession measurements for the encapsulated bilayer graphene device. These two devices are adjacent and share the same bilayer graphene and BN substrate. (**d**) The mobility dependence of the spin-relaxation time.

and hence a spin-relaxation length ($\lambda_S = \sqrt{D_S \tau_S}$) of $\sim 1.3\,\mu$m. We then characterized the adjacent, encapsulated device in the same sample. Clear spin valve and Hanle spin precession signals are obtained in this device as well (Figures 2b and c). For this junction, we extracted a spin-relaxation time of $\tau_S \approx 416$ ps, a spin diffusion constant of $Ds \approx 0.089\,\mathrm{m^2\,s^{-1}}$, and hence a spin-relaxation length of $\lambda s \approx 6.1\,\mu$m, using the same fitting procedure as for the non-encapsulated junction. These measurements indicate four important conclusions. (1) The extracted spin parameters in our non-encapsulated bilayer graphene are comparable with those extracted for bilayer devices on SiO_2 with similar mobilities[11] (inset of Figure 2d and see Supplementary Figure S2). This suggests that substrate-related issues such as roughness, interfacial charged impurities and surface phonons are not the limiting source of spin relaxation in the current devices. (2) Because the encapsulated region is protected against polymer residues during the contact fabrication step, the fivefold enhancement of the spin parameters in the encapsulated device, compared with the non-encapsulated device, suggests that residues have a significant effect on spin transport. (3) The observed enhancement in the encapsulated device compared with the non-encapsulated one suggests that the contacts (~5 kΩ) are not the limiting factor for the spin relaxation. Note that the obtained spin parameters for the encapsulated device should be considered lower bounds because they include the spin transport in the non-encapsulated contact regions. Our observation now allows us to speculate that the observed long spin lifetimes in the study by Drögeler *et al.*[34] may be attributed mainly to the polymer-free fabrication of graphene spin valves rather than only the improvement in contacts. This is also consistent with the observation of a nearly threefold enhancement of an up to 2.7 ns spin-relaxation time in single-layer graphene upon plasma hydrogenation treatment, even when supported on SiO_2, which may be partially attributed to the removal of such residues.[35]

We discuss the origin of the spin-scattering mechanism in bilayer graphene. Figure 2d shows the mobility dependence of the spin-relaxation time, where we observe an increase in the spin-relaxation time as the mobility increases. The increase in mobility is mainly achieved by decreasing the concentration of the impurity. The latter indicates that impurity scattering has a significant role in spin scattering. This contrasts with previous studies, which have demonstrated that although charged impurities affect the carrier mobility, they do not affect spin relaxation.[10,36,37] This suggests that although we are decreasing the concentration of charge scatterers in our devices via the encapsulation process, we are also unintentionally decreasing the source of spin scattering in the device. For instance, this source could be magnetic scatterers that have recently been predicted to increase the spin flipping process without having a significant influence on the charge transport.[27,28] To check the role of the magnetic impurities on spin relaxation, we now investigate the carrier concentration dependence of the local device resistance and

spin-relaxation times in both encapsulated and non-encapsulated devices.

Prior to the carrier concentration-dependent spin transport measurements, we first performed charge characterizations of both encapsulated and non-encapsulated bilayer graphene junctions at room temperature. Our devices are weakly electron doped, which is possibly because of a charge-transfer process from the MgO layer.[11,12] Mobilities of 3600 $cm^2 V s^{-1}$ and 9500 $cm^2 V s^{-1}$ are extracted at room temperature for the non-encapsulated and the encapsulated bilayer graphene, respectively, by using $R = \frac{L}{We\mu\sqrt{n_{res}^2+n^2}}$. Here, μ is the mobility, L and W are the length and width of the channel, respectively, n is the charge-carrier concentration and n_{res} is the residual concentration.[38] We first note that these room temperature mobilities are higher than for similar devices measured on SiO_2 (see refs 9 and 11, and Supplementary Figure S2) and are consistent with previous works using spin valve devices on BN, where a final annealing step is not applied to keep the integrity of the spin-polarized contacts.[8,23,24] It is also important to note that these mobilities are mainly limited by the residues formed during the electrode fabrication process. However, the residue concentration is significantly reduced in the encapsulated junction ($n_{res} = 5.8 \times 10^{11}$ cm^{-2}) compared with that in the non-encapsulated one ($n_{res} = 1.2 \times 10^{12}$ cm^{-2}) because the top BN strip in the encapsulated device protects a large fraction of the junction against polymer contamination.

Figures 3a and b show for the non-encapsulated and encapsulated junctions, respectively, the dependence of the conductivity and spin-relaxation time on the charge-carrier concentration. The strong distortion of the conductance in the hole region is due to the metal–graphene contacts, and is common for spin valve devices.[12,39] Therefore, we limit our analysis mainly to the electron region. We first discuss the low carrier concentration regime ($n < 4 \times 10^{12}$ cm^{-2}), where most of the earlier spin transport measurements were performed. Here, the spin-relaxation time in both the encapsulated and non-encapsulated devices has a monotonic dependence on the carrier concentration. In the non-encapsulated junction, the spin-relaxation time decreases from 250 to 90 ps as the electron-carrier concentration is increased (Figure 3a). Similarly, a decrease from 330 to 260 ps is observed in the encapsulated junction as the carrier concentration is increased in this low carrier concentration regime (Figure 3b). In this study, such scaling is consistently observed in all devices measured both at room temperature and 2.4 K (Supplementary Figures S3), and is similar to what has previously been observed at low temperatures in the lower-mobility bilayer graphene spin valves on an SiO_2 substrate.[9,11] Next, we discuss the spin-relaxation times in the high carrier concentration regime ($n > 4 \times 10^{12}$ cm^{-2}). Near $\sim 4 \times 10^{12}$ cm^{-2}, we observe an upturn in the carrier concentration dependence of the spin-relaxation time in both non-encapsulated and encapsulated junctions (colored region in Figures 3a and b). Remarkably there is no corresponding signature in the charge transport at this carrier concentration. This previously unobserved upturn in the spin lifetime calls into question what the dominant relaxation mechanism in bilayer graphene is. Previous experiments using bilayer graphene on an SiO_2 substrate have attributed the inverse scaling between the spin and momentum relaxation times near $\sim 2 \times 10^{12}$ cm^{-2} to the presence of a Dyakonov–Perel spin-scattering mechanism.[11] However, this low density is below the regime where the upturn in spin-relaxation time is observed; therefore, the scaling at this point can lead to different conclusions. We first note that neither encapsulated or non-encapsulated devices show an inverse relation between the momentum and spin-relaxation times in the low carrier concentration regime, as shown in Figures 3c and d. We also observe a clear increase

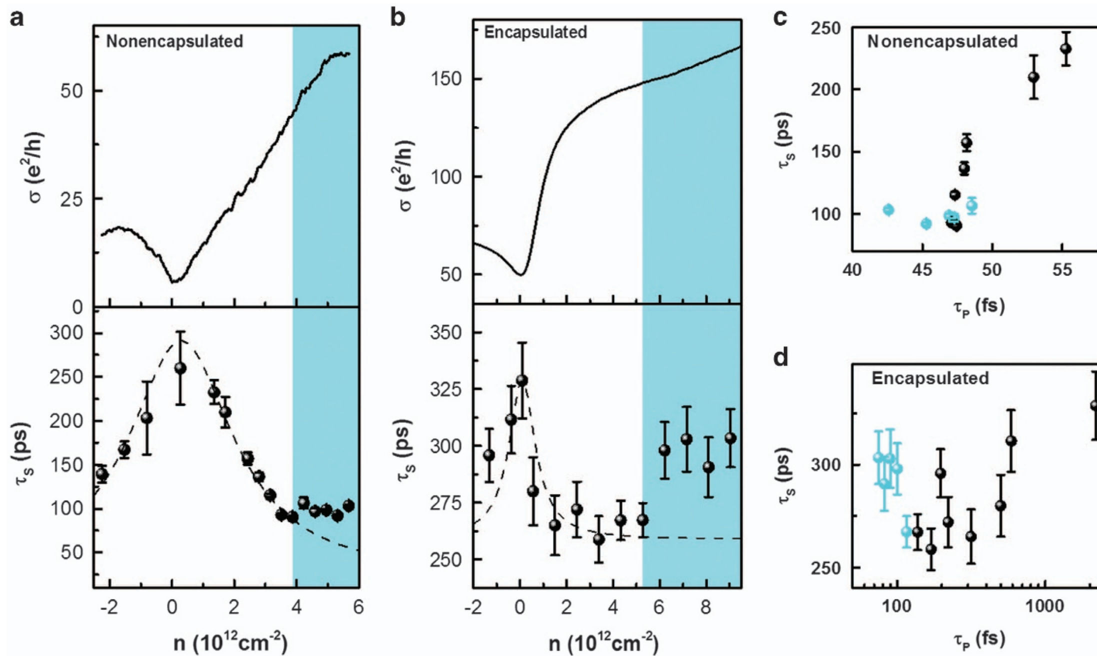

Figure 3 Gate-dependent electronic spin transport measurements. (**a**, **b**) The carrier concentration dependence on the spin-relaxation times for the bilayer graphene-based non-encapsulated and encapsulated spin valves. The non-encapsulated device is measured at 2.4 K. The encapsulated device is measured at RT by varying V_{TG}, whereas V_{BG} is fixed at 25 V. The dotted lines in the bottom panels are a guide to the eye, showing the expected spin-relaxation times without involving the effect of the magnetic resonance. (**c**, **d**) A comparison between the spin- and momentum-scattering times for the devices shown in **a** and **b**. Cyan points represent the high charge-carrier range.

in the spin-relaxation time as the mobility of the device increases (Figure 2d). All of these observations indicate that Dyakonov–Perel spin relaxation is not the dominant mechanism in our devices. However, at higher carrier concentrations, the spin and momentum relaxation times appear to change their dependence and scale inversely. Such dependencies in both low and high carrier concentration regimes appear to agree with the recent theoretical work where the spin relaxation in graphene is proposed to be dominated by resonant scatterers because of the presence of a low concentration of magnetic impurities, such as polymer residues.[27] In that theory, the inverse dependence of the spin relaxation on the carrier concentration in bilayer and single-layer graphene was attributed to the different scales of energy fluctuations in these two systems because of their different density of states. Away from the puddle regime, the sudden increase in spin-relaxation time at $\sim 4\text{–}5\times10^{12}\,\mathrm{cm}^{-2}$, with no corresponding signature in the charge transport, is expected for bilayer graphene because of the scattering from these resonant magnetic scatterers. We remark that, although, our observations serve as an indication of the picture of resonant scattering mentioned above, there is no general agreement on the exact spin-relaxation mechanism in bilayer graphene, and further work is required to elucidate its complex nature.

Now, we turn our attention to the transport across p–n junctions in Sample B. The combination of local V_{TG} and global V_{BG} electrostatic gating allows us to locally control the charge density and carrier type in the channel, and create bipolar junctions between the injector and detector electrodes.[40] For this, V_{TG} was kept fixed at 0 V, -2.5 V and 2.5 V, whereas charge and spin transport measurements were performed as a function of V_{BG}. We first discuss the $V_{TG}=0$ V case. Similar to sample A, the device is slightly electron doped (Figure 4). The extracted electronic mobility at room temperature is $9000\,\mathrm{cm}^2\,\mathrm{Vs}^{-1}$. The room temperature spin-relaxation time and length at $V_{BG}=0$ V are 400 ps and 5.75 μm, respectively. Again, the spin-relaxation time decreases as the carrier concentration is increased. We observe clear pp'p and npn bipolar junctions, whereas V_{BG} is swept at a fixed $V_{TG}=2.5$ V, and pp'p, pnp and nn'n bipolar junctions are observed at $V_{TG}=-2.5$ V. Conversely, the dependence of the spin-relaxation time on the carrier concentration has a very similar behavior as the local device resistance, which is consistent with the response in the low carrier concentration regime discussed above, considering an effective averaging of the channel properties. At present, we do not find strong evidence of significant spin scattering at the pn barriers.

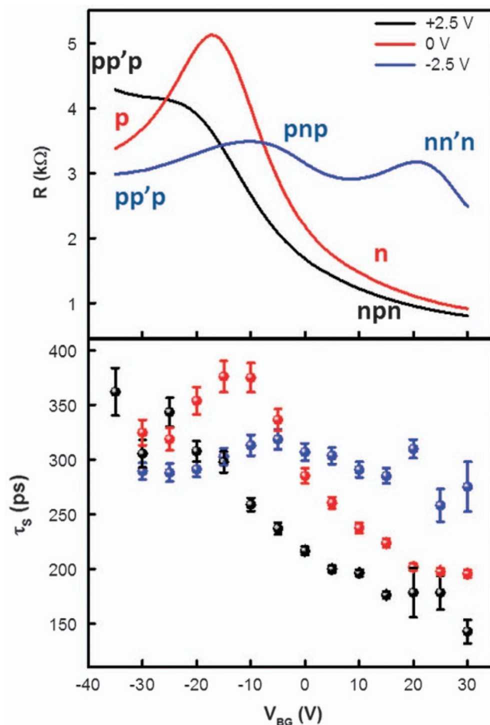

Figure 4 Bipolar electronic spin transport measurements. The V_{BG} dependence on the local device resistance and the spin-relaxation time measured at the fixed V_{TG} values.

Finally, we study the charge and spin transport at a low temperature (2 K). The presence of an on-site energy difference between the bottom and top layer induces a band gap in bilayer graphene.[41] This can be achieved with the application of a vertical electric field through the bilayer graphene plane. Although infrared spectroscopy measurements yield large band gaps of up to 250 meV,[42] the strong role played by disorder limits the expected strong suppression of charge transport measurements and results in only a few meV as the effective transport gap.[43] Figure 5a shows the 2D plot of the local resistance as a function of V_{BG} and V_{TG}. Near the charge neutrality point, the device resistance increases approximately fivefold as the total displacement electric field is increased. This is a direct indication of the induced transport gap.[41] The extracted electronic mobility is $\sim 24\,000\,\mathrm{cm}^2\,\mathrm{Vs}^{-1}$ at 2 K. Next, we study spin transport near the charge neutrality point as the displacement field (D) is increased in our dual-gated device. Figures 5c and d show the spin transport and spin precession measurements as D is increased. At $D\approx0$, we calculate a spin-relaxation length of ~ 9.5 μm. At very small D, we still observe a clear spin signal. The extracted spin-relaxation times and lengths are on the order of ~ 500 ps and ~ 10 μm, respectively, similar to the $D\approx0$ case. This implies that no additional scattering happens at small gaps. However, as D increases, we observe a strong suppression of the spin signal, and eventually the signal becomes comparable with the noise level (~20 mΩ) and undetectable. This prevents us from extracting the spin-relaxation times at large D values. Figure 5b shows the sharp decrease in the spin signal as the local resistance at the charge neutrality point increases. Although a $\Delta R_{NL}\,\alpha\,R^{-1}$ dependence is expected for transparent (pin-hole) contacts in spin valve devices,[33] the observation of a $\Delta R_{NL}\,\alpha\,R^{-3.04}$ dependence suggests the presence of an additional mechanism driving the decrease in the non-local signal. This results in a modulation of more than one order of magnitude purely via electrostatic gating (Figure 5b). We attribute this marked response to the formation of a transport gap in the (encapsulated) dual-gated regions. The highly resistive state in those regions would effectively block diffusion toward the non-local detector of the electronic spin, which tends to remain within the (non-encapsulated) regions where the magnetic contacts are located. This scenario leads us to an interesting case of the spin conductivity mismatch problem,[44] where the regions with large and low spin conductance are both contained within the spin transport channel. We note that the spin signal at room temperature is modulated by only ~ 50 %, confirming the interpretation of a strong modulation only when a sizable transport gap is present (Supplementary Figure S6).

CONCLUSION

Here, we report on spin transport in high-mobility bilayer graphene spin valve devices encapsulated by BN. The effect of a transport gap and pn junctions on spin transport is discussed. Our comparative

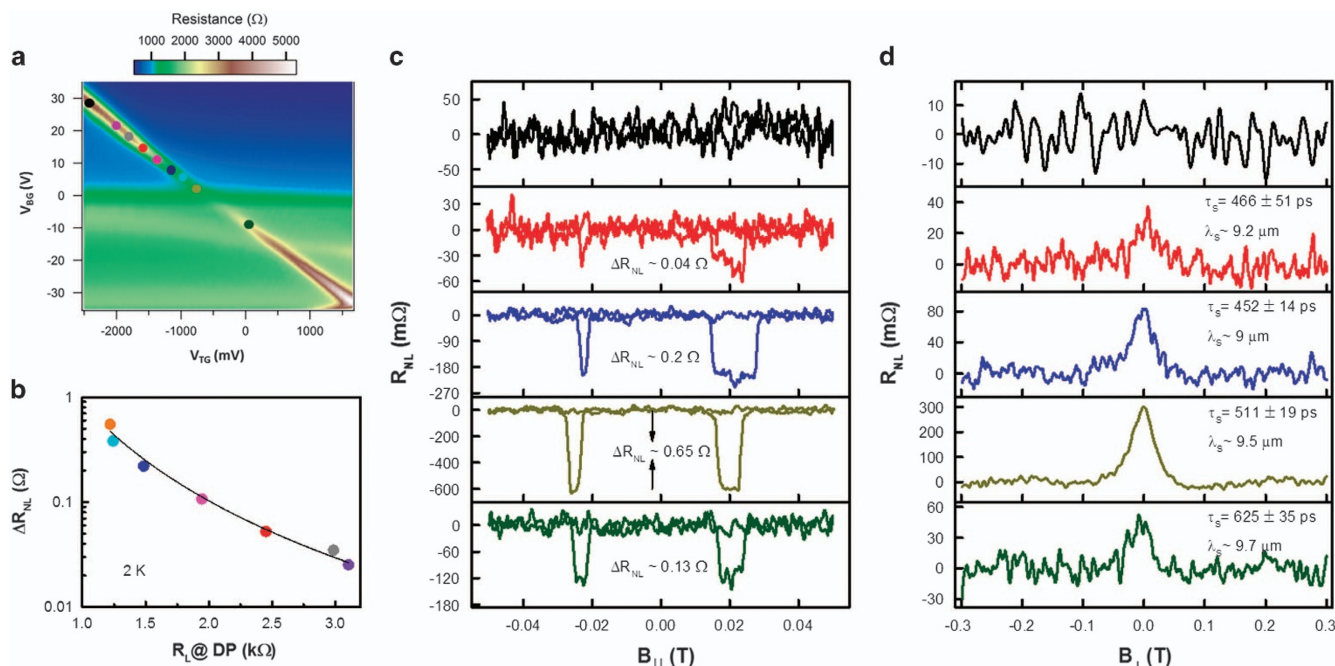

Figure 5 Electronic spin transport measurements in the presence of a transport gap at 2 K. (**a**) A 2D color plot of the local device resistance as a function of V_{TG} and V_{BG}. The device resistance at the Dirac point shows a fivefold increase because of the induced band gap. (**b**) The spin signal diminishes very rapidly as the transport gap is increased. The black line is the fit for the experimental data points. (**c**, **d**) The spin transport and precession measurements at various displacement fields. The measurement points are highlighted in the 2D color plot with their corresponding colors.

study suggests that substrate and contacts are not the key limiting factors for spin relaxation; rather, it pinpoints the role of polymer residues or ambient adsorbates. We achieve spin-relaxation lengths of ~6 μm and ~10 μm at RT and 2 K, respectively. The carrier concentration dependence on the spin-relaxation time seems to be in good agreement with the resonant scattering-based spin-scattering theory. Our flexible device architecture offers the prospect of a further enhancement of the extracted spin transport parameters by allowing the optimization of the length of both the encapsulated and the contact regions.

CONFLICT OF INTEREST

The authors declare no conflict of interest.

ACKNOWLEDGEMENTS

BÖ acknowledges support by the National Research Foundation, Prime Minister's Office, Singapore, under its Competitive Research Program (CRP Award No. NRF-CRP9-2011-3), the Singapore National Research Foundation Fellowship award (RF2008-07, NRF-NRFF2012-01), and the SMF-NUS Research Horizons Award 2009-Phase II. IJVM acknowledges support by The Netherlands Organization for Scientific Research (NWO) and the Future and Emerging Technologies (FET) programme within the Seventh Framework Programme for Research of the European Commission, under FET-Open Grant No. 618083 (CNTQC). We thank S Roche, J Fabian, T Taychatanapat, Y Yeo, I Yudhistira and S Natarajan for their help and useful discussions.

1 Han, W., Kawakami, R. K., Gmitra, M. & Fabian, J. Graphene spintronics. *Nat. Nanotechnol.* **9**, 794–807 (2014).
2 Geim, A. K. Graphene: status and prospects. *Science* **324**, 1530–1534 (2009).
3 Konschuh, S., Gmitra, M. & Fabian, J. Tight-binding theory of the spin-orbit coupling in graphene. *Phys. Rev. B* **82**, 245412 (2010).
4 Huertas-Hernando, D., Guinea, F. & Brataas, A. Spin-orbit coupling in curved graphene, fullerenes, nanotubes, and nanotube caps. *Phys. Rev. B* **74**, 155426 (2006).
5 Trauzettel, B., Bulaev, D. V., Loss, D. & Burkard, G. Spin qubits in graphene quantum dots. *Nat. Phys.* **3**, 192–196 (2007).
6 Wojtaszek, M., Vera-Marun, I. J., Whiteway, E., Hilke, M. & van Wees, B. J. Absence of hyperfine effects in 13 C-graphene spin-valve devices. *Phys. Rev. B* **89**, 035417 (2014).
7 Tombros, N., Jozsa, C., Popinciuc, M., Jonkman, H. T. & van Wees, B. J. Electronic spin transport and spin precession in single graphene layers at room temperature. *Nature* **448**, 571–574 (2007).
8 Zomer, P. J., Guimarães, M. H. D., Tombros, N. & van Wees, B. J. Long-distance spin transport in high-mobility graphene on hexagonal boron nitride. *Phys. Rev. B* **86**, 161416 (2012).
9 Han, W. & Kawakami, R. K. Spin relaxation in single-layer and bilayer graphene. *Phys. Rev. Lett.* **107**, 047207 (2011).
10 Pi, K., Han, W., McCreary, K. M., Swartz, A. G., Li, Y. & Kawakami, R. K. Manipulation of spin transport in graphene by surface chemical doping. *Phys. Rev. Lett.* **104**, 187201 (2010).
11 Yang, T.-Y., Balakrishnan, J., Volmer, F., Avsar, A., Jaiswal, M., Samm, J., Ali, S. R., Pachoud, A., Zeng, M., Popinciuc, M., Güntherodt, G., Beschoten, B. & Özyilmaz, B. Observation of long spin-relaxation times in bilayer graphene at room temperature. *Phys. Rev. Lett.* **107**, 047206 (2011).
12 Avsar, A., Yang, T.-Y., Bae, S., Balakrishnan, J., Volmer, F., Jaiswal, M., Yi, Z., Ali, S. R., Güntherodt, G., Hong, B. H., Beschoten, B. & Özyilmaz, B. Toward wafer scale fabrication of graphene based spin valve devices. *Nano Lett.* **11**, 2363–2368 (2011).
13 Maassen, T., van den Berg, J. J., Ijbema, N., Fromm, F., Seyller, T., Yakimova, R. & van Wees, B. J. Long spin relaxation times in wafer scale epitaxial graphene on SiC(0001). *Nano Lett.* **12**, 1498–1502 (2012).
14 Dlubak, B., Martin, M.-B., Deranlot, C., Servet, B., Xavier, S., Mattana, R. *et al.* Highly efficient spin transport in epitaxial graphene on SiC. *Nat. Phys.* **8**, 557–561 (2012).
15 Kamalakar, M. V., Groenveld, C., Dankert, A. & Dash, S. P. Long distance spin communication in chemical vapour deposited graphene. *Nat. Commun.* **6**, 6766 (2015).
16 Ertler, C., Konschuh, S., Gmitra, M. & Fabian, J. Electron spin relaxation in graphene: the role of the substrate. *Phys. Rev. B* **80**, 041405 (2009).
17 Guimarães, M. H. D., Veligura, A., Zomer, P. J., Maassen, T., Vera-Marun, I. J., Tombros, N. & van Wees, B. J. Spin transport in high-quality suspended graphene devices. *Nano Lett.* **12**, 3512–3517 (2012).
18 Dean, C. R., Young, A. F., Meric, I., Lee, C., Wang, L., Sorgenfrei, S., Watanabe, K., Taniguchi, T., Kim, P., Shepard, K. L. & Hone, J. Boron nitride substrates for high-quality graphene electronics. *Nat. Nanotechnol.* **5**, 722–726 (2010).
19 Tan, J. Y., Avsar, A., Balakrishnan, J., Koon, G. K. W., Taychatanapat, T., O'Farrell, E. C. T. *et al.* Electronic transport in graphene-based heterostructures. *Appl. Phys. Lett.* **104**, 183504 (2014).
20 Zomer, P. J., Dash, S. P., Tombros, N. & van Wees, B. J. A transfer technique for high mobility graphene devices on commercially available hexagonal boron nitride. *Appl. Phys. Lett.* **99**, 232104 (2011).

21 Mayorov, A. S., Gorbachev, R. V., Morozov, S. V., Britnell, L., Jalil, R., Ponomarenko, L. A., Blake, P., Novoselov, K. S., Watanabe, K., Taniguchi, T. & Geim, A. K. Micrometer-scale ballistic transport in encapsulated graphene at room temperature. *Nano Lett.* **11**, 2396–2399 (2011).
22 Wang, L., Meric, I., Huang, P. Y., Gao, Q., Gao, Y., Tran, H., Taniguchi, T., Watanabe, K., Campos, L. M., Muller, D. A., Guo, J., Kim, P., Hone, J., Shepard, K. L. & Dean, C. R. One-dimensional electrical contact to a two-dimensional material. *Science* **342**, 614–617 (2013).
23 Guimarães, M. H. D., Zomer, P. J., Ingla-Aynés, J., Brant, J. C., Tombros, N. & van Wees, B. J. Controlling spin relaxation in hexagonal BN-encapsulated graphene with a transverse electric field. *Phys. Rev. Lett.* **113**, 086602 (2014).
24 Ingla-Aynés, J., Guimarães, M. H. D., Meijerink, R. J., Zomer, P. J. & van Wees, B. J. 24 μm spin relaxation length in boron nitride encapsulated bilayer graphene. *Phys. Rev. B* **92**, 201410 (2015).
25 Dyakonov, M. & Perel, V. Spin relaxation of conduction electrons in noncentrosymmetric semiconductors. *Sov. Phys. Solid State* **13**, 3023 (1972).
26 Konschuh, S., Gmitra, M., Kochan, D. & Fabian, J. Theory of spin-orbit coupling in bilayer graphene. *Phys. Rev. B* **85**, 115423 (2012).
27 Kochan, D., Irmer, S., Gmitra, M. & Fabian, J. Resonant scattering by magnetic impurities as a model for spin relaxation in bilayer graphene. *Phys. Rev. Lett.* **115**, 196601 (2015).
28 Kochan, D., Gmitra, M. & Fabian, J. Spin relaxation mechanism in graphene: resonant scattering by magnetic impurities. *Phys. Rev. Lett.* **112**, 116602 (2014).
29 Van Tuan, D., Ortmann, F., Soriano, D., Valenzuela, S. O. & Roche, S. Pseudospin-driven spin relaxation mechanism in graphene. *Nat. Phys.* **10**, 857–863 (2014).
30 Castro Neto, A. & Guinea, F. Impurity-induced spin-orbit coupling in graphene. *Phys. Rev. Lett.* **103**, 026804 (2009).
31 Van Tuan, D., Ortmann, F., Cummings, A. W., Soriano, D. & Roche, S. Spin dynamics and relaxation in graphene dictated by electron-hole puddles. *Sci. Rep.* **6**, 21046 (2016).
32 Avsar, A., Tan, J. Y., Taychatanapat, T., Balakrishnan, J., Koon, G. K. W., Yeo, Y., Lahiri, J., Carvalho, A., Rodin, A. S., O'Farrell, E. C., Eda, G., Castro Neto, A. H. & Özyilmaz, B. Spin-orbit proximity effect in graphene. *Nat. Commun.* **5**, 4875 (2014).
33 Han, W., Pi, K., McCreary, K. M., Li, Y., Wong, J. J. I., Swartz, A. G. & Kawakami, R. K. Tunneling spin injection into single layer graphene. *Phys. Rev. Lett.* **105**, 167202 (2010).
34 Drögeler, M., Volmer, F., Wolter, M., Terrés, B., Watanabe, K., Taniguchi, T., Güntherodt, G., Stampfer, C. & Beschoten, B. Nanosecond spin lifetimes in single- and few-layer graphene-hBN heterostructures at room temperature. *Nano Lett.* **14**, 6050–6055 (2014).
35 Wojtaszek, M., Vera-Marun, I. J., Maassen, T. & van Wees, B. J. Enhancement of spin relaxation time in hydrogenated graphene spin-valve devices. *Phys. Rev. B* **87**, 081402 (2013).
36 Han, W., Chen, J.-R., Wang, D., McCreary, K. M., Wen, H., Swartz, A., Shi, J. & Kawakami, R. K. Spin relaxation in single-layer graphene with tunable mobility. *Nano Lett.* **12**, 3443–3447 (2012).
37 Lundeberg, M. B., Yang, R., Renard, J. & Folk, J. A. Defect-mediated spin relaxation and dephasing in graphene. *Phys. Rev. Lett.* **110**, 156601 (2013).
38 Kim, S., Nah, J., Jo, I., Shahrjerdi, D., Colombo, L., Yao, Z. *et al.* Realization of a high mobility dual-gated graphene field-effect transistor with Al2O3 dielectric. *Appl. Phys. Lett.* **94**, 062107 (2009).
39 Nouchi, R. & Tanigaki, K. Charge-density depinning at metal contacts of graphene field-effect transistors. *Appl. Phys. Lett.* **96**, 253503 (2010).
40 Özyilmaz, B., Jarillo-Herrero, P., Efetov, D., Abanin, D. A., Levitov, L. S. & Kim, P. Electronic transport and quantum hall effect in bipolar graphene p—n—p Junctions*Phys. Rev. Lett.* **99**, 166804 (2007).
41 Oostinga, J. B., Heersche, H. B., Liu, X., Morpurgo, A. F. & Vandersypen, L. M. K. Gate-induced insulating state in bilayer graphene devices. *Nat. Mater.* **7**, 151–157 (2008).
42 Zhang, Y., Tang, T.-T., Girit, C., Hao, Z., Martin, M. C., Zettl, A., Crommie, M. F., Shen, Y. R. & Wang, F. Direct observation of a widely tunable bandgap in bilayer graphene. *Nature* **459**, 820–823 (2009).
43 Taychatanapat, T. & Jarillo-Herrero, P. Electronic transport in dual-gated bilayer graphene at large displacement fields. *Phys. Rev. Lett.* **105**, 166601 (2010).
44 Maassen, T., Vera-Marun, I. J., Guimarães, M. H. D. & van Wees, B. J. Contact-induced spin relaxation in Hanle spin precession measurements. *Phys. Rev. B* **86**, 235408 (2012).

This work is licensed under a Creative Commons Attribution 4.0 International License. The images or other third party material in this article are included in the article's Creative Commons license, unless indicated otherwise in the credit line; if the material is not included under the Creative Commons license, users will need to obtain permission from the license holder to reproduce the material. To view a copy of this license, visit http://creativecommons.org/licenses/by/4.0/

Supplementary Information accompanies the paper on the NPG Asia Materials website (http://www.nature.com/am)